LETTERS

Warming trends in Asia amplified by brown cloud solar absorption

Veerabhadran Ramanathan[1], Muvva V. Ramana[1], Gregory Roberts[1], Dohyeong Kim[1], Craig Corrigan[1], Chul Chung[1] & David Winker[2]

Atmospheric brown clouds are mostly the result of biomass burning and fossil fuel consumption[1]. They consist of a mixture of light-absorbing and light-scattering aerosols[1] and therefore contribute to atmospheric solar heating and surface cooling. The sum of the two climate forcing terms—the net aerosol forcing effect—is thought to be negative and may have masked as much as half of the global warming attributed to the recent rapid rise in greenhouse gases[2]. There is, however, at least a fourfold uncertainty[2] in the aerosol forcing effect. Atmospheric solar heating is a significant source of the uncertainty, because current estimates are largely derived from model studies. Here we use three lightweight unmanned aerial vehicles that were vertically stacked between 0.5 and 3 km over the polluted Indian Ocean. These unmanned aerial vehicles deployed miniaturized instruments measuring aerosol concentrations, soot amount and solar fluxes. During 18 flight missions the three unmanned aerial vehicles were flown with a horizontal separation of tens of metres or less and a temporal separation of less than ten seconds, which made it possible to measure the atmospheric solar heating rates directly. We found that atmospheric brown clouds enhanced lower atmospheric solar heating by about 50 per cent. Our general circulation model simulations, which take into account the recently observed widespread occurrence of vertically extended atmospheric brown clouds over the Indian Ocean and Asia[3], suggest that atmospheric brown clouds contribute as much as the recent increase in anthropogenic greenhouse gases to regional lower atmospheric warming trends. We propose that the combined warming trend of 0.25 K per decade may be sufficient to account for the observed retreat of the Himalayan glaciers[4–6].

Field experiments[1,7] during the past decade over the polluted oceans provided observational constraints for the regional aerosol forcing, but these studies were limited to the vertically integrated forcing of the surface–atmosphere system. Crucial to our understanding of the tropical regions would be direct observations of the vertical heating rate. During the six-month-long tropical dry season, convective coupling between the surface and the troposphere is weak. As a result, aerosol solar heating can amplify the effect of greenhouse gases in warming the atmosphere while simultaneously cooling the surface[1]. The primary motivation for the Maldives Autonomous unmanned aerial vehicle Campaign (MAC), the results of which are reported here, was the observational determination of this solar heating and the examination of its role in atmospheric warming trends.

MAC extends the pioneering lightweight unmanned aerial vehicle (UAV) campaigns initiated by other investigators[8] by stacking three UAVs and synchronizing the heating rate measurements with measurements of aerosols, clouds, humidity and temperature. The

downward and reflected broadband (305 to 2,800 nm) and visible (400 to 700 nm) solar fluxes were measured typically at 0.5, 1.5 and 3 km. The net fluxes (down minus up) were differenced to obtain the heating rate for the layer between the flight levels.

MAC was conducted over the Indian Ocean from the island of Hanimadhoo (6.78° N, 73.18° E) during March 2006. The UAV measurements were validated with identical measurements at the Maldives Climate Observatory at Hanimadhoo (MCOH)[9] during low-altitude overflights. March is part of the dry season (November to May), when low-level flow brings polluted air-mass from Asia to most of the northern Indian Ocean[1]. During 4–16 March (period 1), the air-mass was of marine origin, but was still influenced by atmospheric brown clouds (ABCs) with near-surface aerosol number concentrations as high as 1,000 cm^{-3}. The aerosol layer was confined to the boundary layer (Fig. 1a). During 19–29 March (period 2), MAC detected 1–3-day-old air mass from southern Asia above 1 km (Supplementary Fig. 1). The measured aerosol absorption coefficient above 1 km increased tenfold (Fig. 1a), equivalent to a 700 ng m^{-3} increase of black carbon mass. The aerosol number concentration increased from about 750 to about 2,500 cm^{-3}. The boundary-layer aerosol number concentration was similar to that during period 1. The measured visible aerosol optical depth, AOD, a good index for column-averaged scattering and absorption, was 0.18 during period 1 and 0.4 during period 2. The visible absorption optical depth, AOD$_{abs}$, increased from about 0.005 to 0.027 from periods 1 to 2.

The observed heating rates are shown in Fig. 1b and c together with the simulated values using the Monte Carlo Aerosol Cloud Radiation model (MACR) described elsewhere[1]. MACR used MAC and MCOH data for aerosol and cloud parameters, H_2O and O_3. For the 0.5–3 km layer, the mean period 1 diurnal average heating rates H for MAC and MACR were respectively 1.1($\pm$0.3) and 1.2($\pm$0.3) K per day; the period 2 H values were respectively 1.8($\pm$0.2) and 1.65($\pm$0.2) K per day. The agreement between MAC and MACR demonstrates that it is possible to measure H accurately in the atmosphere using multiple aircraft and link the H value with observations of atmospheric constituents using models. Figure 1d shows the magnitude of the heating that is due to the addition of ABCs from southern Asia: ΔH, the difference in H over 0.5–3 km between the two periods. The ΔH from MACR is about 0.45($\pm$0.3) K per day compared with the MAC value of 0.7($\pm$0.3) K per day. The difference is within experimental and modelling uncertainties. MACR simulations show that about 90% of the ΔH is attributable to soot. The balance is due to small changes in water vapour and clouds. The major role of soot is also confirmed by the increase in heating of about 0.25($\pm$0.15) K per day detected by the visible radiometer. Elemental and organic carbon in soot are the dominant absorbers[10,11] in the visible wavelengths. In

[1]Center for Clouds, Chemistry and Climate, Scripps Institution of Oceanography, UCSD, La Jolla, California 92037, USA. [2]NASA Langley Research Center, Hampton, Virginia 23681-0001, USA.

addition, direct measurements of elemental carbon mass from filter samples at MCOH correlated strongly[12] with the measured aerosol absorption coefficient. Our main deduction from Fig. 1d is that ABCs from southern Asia increased AOD and AOD_{abs} respectively by 0.22 and 0.02, which was sufficient to enhance H by about 50%. This plume is part of the widespread ABC that envelops most of Asia and the adjacent oceans, as documented extensively[1,13,14]. Hence the UAV-measured large solar heating rates have climatic implications, which we consider below.

In what follows, we will rely on the estimates of Chung et al.[14], because this study used both satellite and ground-based observations to account for the spatial and temporal variations of ABCs. AODs, solar heating and surface dimming were obtained for the period from 2000 to 2003 (ref. 14). The monthly AOD (and AOD_{abs}) values over India varied from 0.1 (and 0.01) in July to 0.3 (and 0.03) during January, whereas over China they increased from 0.1 (and 0.01) in January to 0.35 (and 0.04) in July (Supplementary Fig. 2). Comparing these with the MAC AOD values and ΔH, we conclude that ABCs can enhance the solar heating rates substantially on spatio-temporal scales relevant for climate impact studies. The impact on climate depends also on the vertical extent of the plume[1], but such data were unavailable until recently.

The vertical extent data are now available through the Cloud Aerosol Lidar and Infrared Pathfinder Satellite (CALIPSO)[3], launched on April 2006. CALIPSO reveals that vertically extended ABCs are widespread through most of southern and eastern Asia (Fig. 2) with peak lidar (light detection and ranging) returns of between 1 to 3 km above sea level (a.s.l.), which is indicative of aerosol concentrations and is similar to the MAC vertical extent (Fig. 1a). The 1–3 km a.s.l. plume is persistent from November 2006 to March 2007 (Fig. 2a–d and Supplementary Fig. 3) over the region of interest.
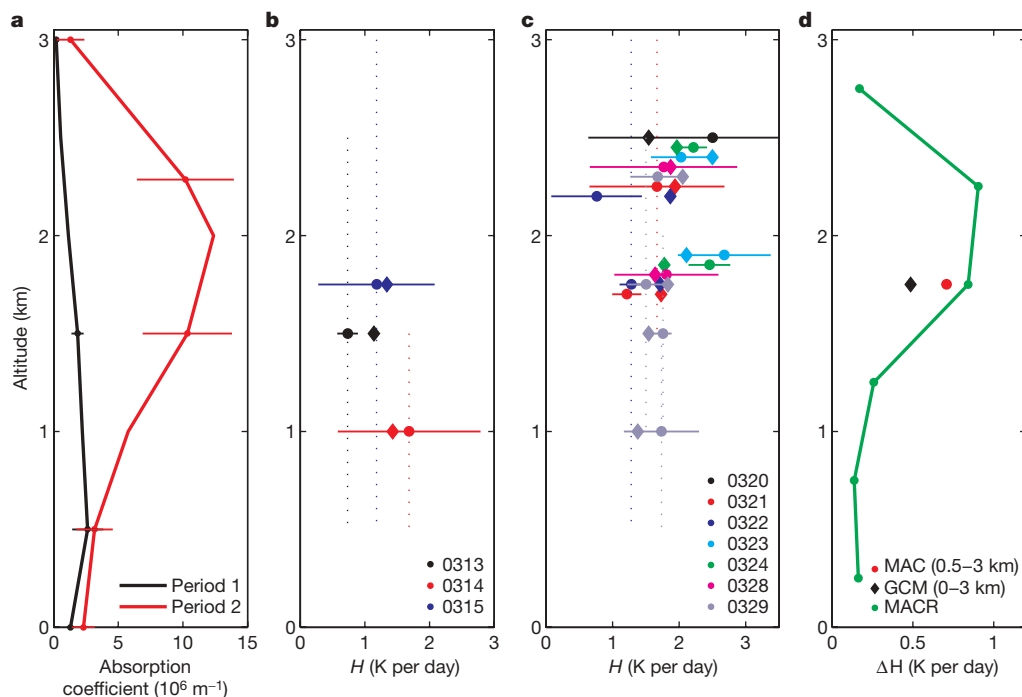
Using aircraft data over the Indian Ocean[1], Chung et al.[14] assumed that ABCs extended to 3 km a.s.l. over Asia, and this assumption is now supported by the CALIPSO data. Because the AOD and AOD_{abs} values were also constrained by observations, their forcing values provide a sound starting point for evaluating the climate impacts. For example, the 0–3 km layer heating per unit AOD_{abs} from MAC (Fig. 1d) is about 32 K per day per unit AOD_{abs} compared with the ref. 14 value of 23 K per day per unit AOD_{abs}. We inserted monthly mean ABC solar heating rates[14] (Supplementary Fig. 4) and dimming in the CCM3 version[15] of the NCAR general circulation model (GCM) and conducted simulations (see Methods).

The tropical average model atmosphere warms in response to the imposed ABC heating, with peak annual mean warming of 0.4 K between 2 and 4 km a.s.l. (Supplementary Fig. 5). The annual warming at 700 mb (about 3 km a.s.l.) over the Himalayan-Hindu-Kush region is about 0.6 K (Fig. 3), with peak warming during March to September (Supplementary Fig. 6). Although ABC heating is restricted to the lower troposphere (pressure $P > 700$ mb), the warming penetrates well into the mid-troposphere (500 mb) owing to vertical transport (Supplementary Fig. 7).

As reported in ref. 16, emissions of the ABC precursors SO_2 and soot increased tenfold from 1930 to 2000. Using these emissions data, it has been shown[13] that more than 90% of the simulated ABC aerosol forcing and the induced atmospheric warming is attributable to the period from 1950 to present. We obtained the lower atmosphere warming simulated by the NCAR model for the greenhouse gas forcing for 1950 to 2000 (ref. 17). For the 2 to 5 km (a.s.l.) layer, this warming is about 0.5–0.8 K. The ratio of the ABC warming and the 1950–2000 greenhouse gas warming is about 1 over the Himalayan-Hindu-Kush region (Supplementary Fig. 7). The combined simulated warming of greenhouse gases and ABCs at the higher levels (3–5 km a.s.l.) is about 1.2 K, or about 0.25 K per decade during

Figure 1 | Vertical distribution of UAV observations. The MAC period is divided into two periods. Period 1 covers 4–16 March, when aerosol was mainly below 1 km; period 2 covers 19–29 March, when aerosol was elevated. **a**, Aerosol absorption coefficient. **b**, Diurnally averaged solar heating rate H for period 1. The instantaneous fluxes were normalized to diurnal average solar fluxes using MACR simulations to obtain diurnal mean H. The vertical bar shows the layer depth; the horizontal bar shows the variations between flight legs, with each flight lasting about 25 min; solid circles are observed values and diamonds are simulated values by MACR. The observation dates are shown (for example 0313 denotes 13 March). **c**, As for **b** but for period 2. **d**, Difference in the vertically (0.5–3 km) averaged H between period 2 and period 1. The green line is the MACR profile for ΔH. The spatial average over the Indian Ocean and southern Asia of the specified CCM3 ABC heating is also shown (GCM). The uncertainty in H is 0.3 K per day for period 1 and 0.2 K per day for period 2. All uncertainty estimates, including those in the text, are 2σ values.
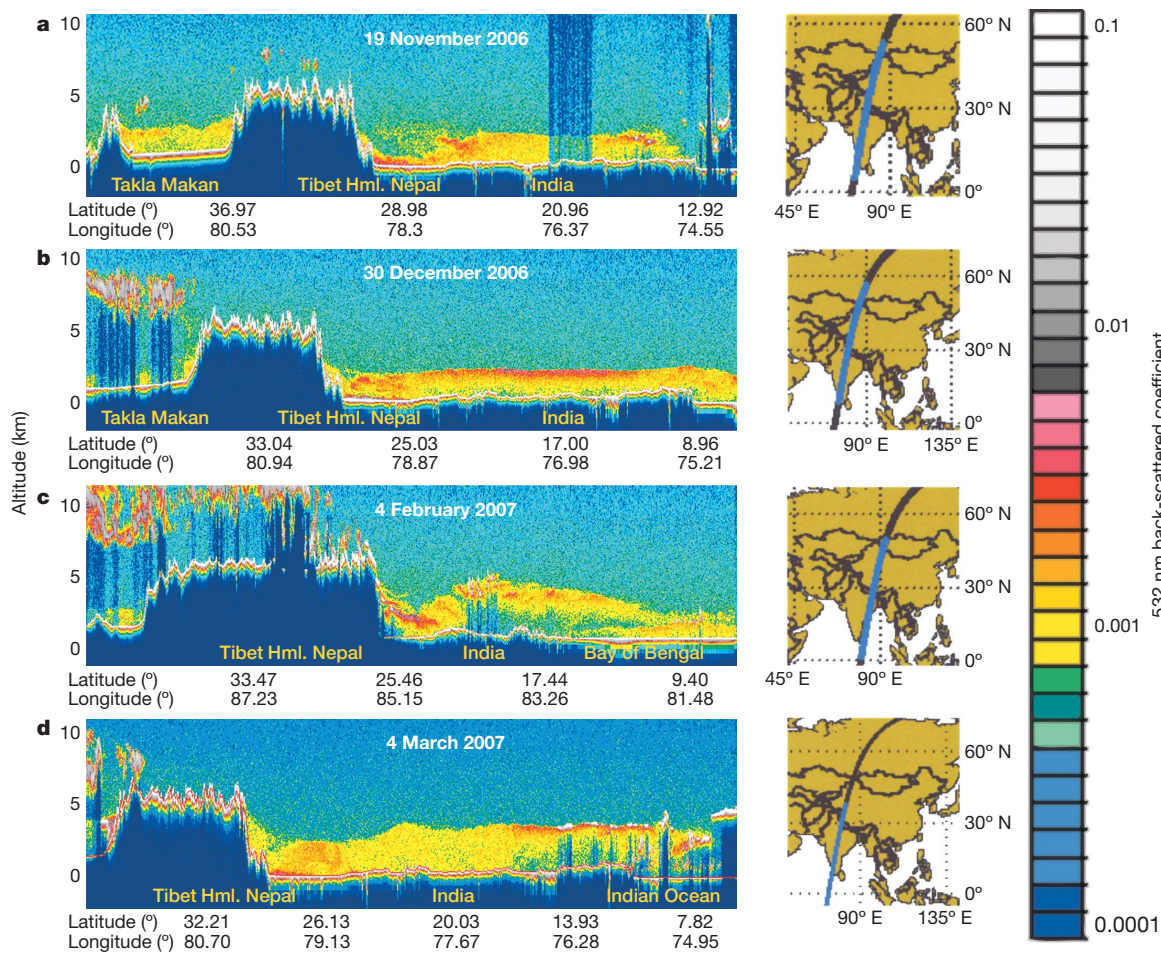
Figure 2 | Colour-coded profiles of 532 nm backscatter return signal from the CALIPSO lidar showing the vertical distribution of ABCs. The panels on the right show the orbit track across Asia and on the left the vertical extent of the aerosol is shown for the blue-shaded portion of each track. We chose the colour scale so that aerosol usually shows up in green, yellow and red (for low, medium and high loadings, respectively) and boundary layer clouds usually show up as grey or white. Cirrus usually ranges from yellow to grey. Sample profiles are shown for four months of the dry season that extends from November to May. The Takla Makan desert is in northwestern China between 37° N and 41° N and 77° E to 90° E. Hml., Himalayas.
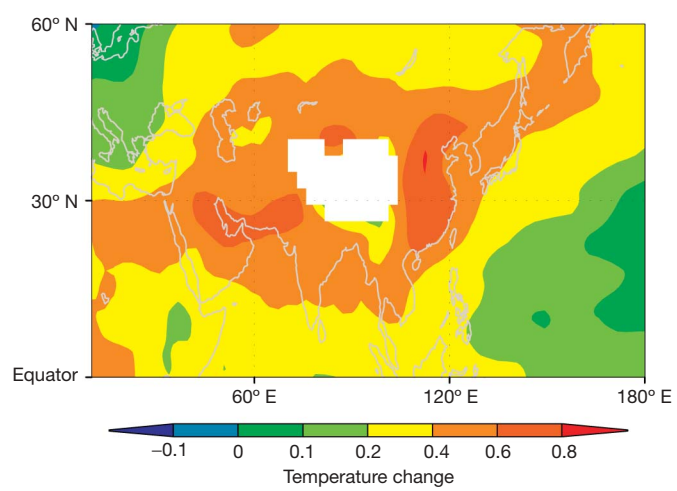
the period from 1950 to present, which is about twice the simulated surface warming trend (Supplementary Figs 5 and 6). This result is also supported by satellite microwave temperature trends from 1979 to 2000 that reveal that the atmospheric trend is larger than the surface trend by about 0.15 K per decade[13] (Supplementary Fig. 8).

The above model results have significant implications because the observed air-temperature trend over the elevated Himalayas has accelerated to between 0.15–0.3 K per decade[18] during the past several decades. This large trend is thought to be the major cause for the Himalayan-Hindu-Kush glacier ablation[5]. The Himalayan-Hindu-Kush region has seen a marked retreat in the glaciers that serve major Asian rivers such as the Yangtze, the Indus and the Ganges[4,19]. The rapid melting of these glaciers, the third-largest ice mass on the planet, if it becomes widespread and continues for several more decades, will have unprecedented downstream effects on southern and eastern Asia[4,5].

METHODS SUMMARY

MAC. The MAC campaign, platforms and instruments are described in ref. 20. The miniaturized instruments are described in ref. 21. The radiation and aerosol instrument measurements were validated with MCOH measurements[22,23]. The overall MAC observations have also been presented[24]. The cloud fraction, measured from the in-cloud UAV cloud droplet instrument, was 11% for period 1 and 5% for period 2. The water vapour amount from 0 to 3 km was 35.1 kg m^{-2} for period 1 and 34.3 kg m^{-2} for period 2.

MACR. Sensitivity studies with MACR were used to understand the factors contributing to ΔH. Because changes in cloud fraction and water vapour amount

Figure 3 | The temperature change dT due to ABC solar heating at the 700 hPa (or 700 mb) level (~3 km a.s.l.) simulated by CCM3. The change is estimated from a 50-year average of experiment and control. The standard error of the mean difference is 0.05 K. All altitudes mentioned in the text are a.s.l. altitudes. For example, a warming of 0.6 K at 3 km a.s.l. would denote near-surface warming for a location in the Himalayas that is at an elevation of 3 km a.s.l. The white-shaded regions are the part of the Himalayas with surface pressure less than 700 mb, that is, surface elevations are higher than 3 km.

between the two periods were small (see above), the net effect of these two parameters on ΔH was only $+0.05 \, \text{K}$ per day. About 10–12% of ΔH was in wavelengths $\lambda < 400 \, \text{nm}$; 37% to 44% for $400 < \lambda < 700 \, \text{nm}$ and 45% to 54% for $\lambda > 700 \, \text{nm}$. Soot contributed 100% of the increased absorption for $\lambda < 700 \, \text{nm}$ and about 70% for $\lambda > 700 \, \text{nm}$.

CCM3. The CCM3 is run with prescribed sea surface temperatures. Chung *et al.*[14] distributed the AOD uniformly from the surface to about 3 km. The solar heating would have been larger by about 50% had we adopted an elevated plume (as in Fig. 1a) instead of the uniform aerosol profile. To compare the ABC warming with that due to the observed warming of the sea surface, we prescribed the observed sea surface temperature trend for the 1950 to 2002 period for each grid point in the model as a function of the month, and ran the model with and without the prescribed aerosol forcing. Four ensemble runs of 52 years each were conducted for the control and the experiments.

Full Methods and any associated references are available in the online version of the paper at www.nature.com/nature.

1. Ramanathan, V. *et al.* Indian Ocean experiment: An integrated analysis of the climate forcing and effects of the great Indo-Asian haze. *J. Geophys. Res.* **106**, doi:10.1029/2001JD900133 (2001).
2. Forster, P. *et al.* in *Climate Change 2007: The Physical Science Basis (Contribution of Working Group I to the Fourth Assessment Report of the Intergovernmental Panel on Climate Change)* 131–217 (World Meteorological Organization, Geneva, 2007).
3. Winker, D. M., Vaughan, M. A. & Hunt, W. H. The CALIPSO mission and initial results from CALIOP. In *Lidar Remote Sensing for Environmental Monitoring VII*; *Proc. SPIE* **6409**, 1–8 (2006).
4. Barnett, T. P., Adam, J. C. & Lettenmaier, D. P. Potential impacts of a warming climate on water availability in snow-dominated regions. *Nature* **438**, 303–309 (2005).
5. Thompson, L. G. *et al.* Tropical glacier and ice core evidence of climate changes on annual to millennial time scales. *Clim. Change* **59**, 137–155 (2003).
6. Vuille, M., Bradley, R. S., Werner, M. & Keimig, F. 20th century climate change in the tropical Andes. *Clim. Change* **59**, 75–99 (2003).
7. Haywood, J. *et al.* Radiative properties and direct radiative effect of Saharan dust measured by the C-130 aircraft during SHADE: 1. Solar spectrum. *J. Geophys. Res.* **108**, doi:10.1029/2002JD002687 (2003).
8. Holland, G. H. *et al.* The aerosonde robotic aircraft: A new paradigm for environmental observations. *Bull. Am. Meteorol. Soc.* **82**, 889–901 (2001).
9. Ramana, M. V. & Ramanathan, V. Abrupt transition from natural to anthropogenic aerosol radiative forcing: Observations at the ABC-Maldives Climate Observatory. *J. Geophys. Res.* **111**, doi:10.1029/2006JD007063 (2006).
10. Andrea, M. O. & Gelencser, A. Black carbon or brown carbon? The nature of light absorbing carbonaceous aerosols. *Atmos. Chem. Phys* **6**, 3131–3148 (2006).
11. Ramaswamy, V. *et al.* in *Climate Change 2001: The Scientific Basis (Contribution of Working Group I to the Third Assessment Report of the Intergovernmental Panel on Climate Change)* (Cambridge Univ. Press, Cambridge, UK, 2001).
12. Corrigan, C. E., Ramanathan, V. & Schauer, J. J. Impact of monsoon transitions on the physical and optical properties of aerosols. *J. Geophys. Res.* **111**, doi:10.1029/2005JD006370 (2006).
13. Ramanathan, V. *et al.* Atmospheric brown clouds: impacts on south Asian climate and hydrological cycle. *Proc. Natl Acad. Sci. USA* **102**, 5326–5333 (2005).
14. Chung, C. E., Ramanathan, V., Kim, D. & Podgorny, I. A. Global anthropogenic aerosol direct forcing derived from satellite and ground-based observations. *J. Geophys. Res.* **110**, doi:10.1029/2005JD006356 (2005).
15. Kiehl, J. T. *et al.* The National Center for Atmospheric Research Community Climate Model: CCM3. *J. Clim.* **11**, 1131–1149 (1998).
16. Novakov, T. *et al.* Large historical changes of fossil-fuel black carbon aerosols. *Geophys. Res. Lett.* **30**, doi:10.1029/2002GL016345 (2003).
17. Washington, W. M. *et al.* Parallel climate model (PCM) control and transient simulations. *Clim. Dyn.* **16**, 755–774 (2000).
18. Liu, X. D. & Chen, B. D. Climatic warming in the Tibetan plateau during recent decades. *Int. J. Climatol.* **20**, 1729–1742 (2000).
19. Kulkarni, A. V., Rathore, B. P., Mahajan, S. & Mathur, P. Alarming retreat of Parbati glacier, Beas basin, Himachal Pradesh. *Curr. Sci.* **88**, 1844–1850 (2005).
20. Ramanathan, V., Roberts, G., Corrigan, C., Ramana, M. V. & Nguyen, H. *Maldives AUAV Campaign (MAC): Observing Aerosol-Cloud-Radiation Interactions Simultaneously from Three Stacked Autonomous Unmanned Aerial Vehicles (AUAVs).* <http://www-abc-asia.ucsd.edu/MAC/ MAC_proposal_FINAL_2005July05.pdf> (2005).
21. Roberts, G. C., Ramanathan, V., Corrigan, C. & Ramana, M. V. Aerosol, cloud, and radiometric measurements with small autonomous unmanned aerial vehicles. *Am. Assoc. Aerosol Res. Conf. (Austin, Texas, 2005)* ⟨http://www-abc-asia.ucsd.edu/MAC/RobertsAAARC2005.pdf⟩ (2005).
22. Ramana, M. V. *et al.* Direct measurements of albedo and solar absorption over the Northern Indian Ocean with a new observing system of stacked multiple AUAVs. *Eos* **87** (52), abstr. A13B–0921 (2006).
23. Corrigan, C. E., Ramanathan, V., Ramana, M. V., Kim, D. & Roberts, G. Vertical profiles of aerosols using unmanned aerial vehicles. *Int. Aerosol Conf.* (St Paul, Minnesota, 2006) ⟨http://www-abc-asia.ucsd.edu/MAC/ Corrigan_IAC_20062.pdf⟩ (2006).
24. Ramanathan, V. *et al.* Simultaneous observations of aerosols, clouds, and radiometric fluxes using light-weight autonomous UAVS. *Eos* **87** (52), abstr. A33B–1007 (2006) <http://www-abc-asia.ucsd.edu/MAC/ RamanathanAGU2006SimultaneousAbstract.pdf>.
25. Dubovik, O. *et al.* Accuracy assessment of aerosol optical properties retrieved from Aerosol Robotic Network (AERONET) sun and sky radiance measurements. *J. Geophys. Res.* **105**, 9791–9806 (2000).

METHODS

UAVs. The UAV is the Manta aircraft built by Advanced Ceramics Research (Arizona, USA). The below-cloud UAV flew below the trade cumulus cloud base at about 0.5 km and the above-cloud UAV flew mostly at 3 km; both UAVs measured boundary-layer aerosol number concentration, size distribution and absorption coefficient at 370, 520 and 880 nm to determine concentration of absorbing aerosols. Up- and down-looking broadband (305 to 2,800 nm) pyranometers (Kipp & Zonen) and visible-band (400–700 nm) radiometers (LICOR) measured the transmitted (from above) and reflected (from below) solar fluxes. The in-cloud UAV flying through the middle of the cloud, typically at about 750 m to 1 km, measured cloud drop number size distribution from 2 to 50 μm in diameter. The instruments and the power supply together weighed 3.5–5.4 kg. When the wind vertical shear was less than 25 m s^{-1}, the UAVs were able to maintain their altitudes and their designed vertical and horizontal separation.

Validation with MCOH. This ground-based observatory[9,12] has been collecting data since 2004. It contains aerosol and radiation instruments identical to those on the UAVs and each flight included a low-level flight within 5 km of MCOH. The aerosol number concentration from the UAVs (below 0.5 km) and the absorption coefficient agreed with MCOH observations within about 10% (ref. 23). The radiometers were validated by two independent methods. We flew two UAVs side by side: the radiometers in the two UAVs agreed within 5 W m^{-2} (0.5%). Next, we conducted fly-bys over the MCOH and the UAV radiometer agreed with the MCOH radiometers[22] within 5 W m^{-2}. The AOD and the AOD$_{abs}$ at 520 nm were measured by the AERONET–CIMEL Sun photometer[25].

MACR simulations. The input to MACR was AERONET data for AOD, AOD$_{abs}$, and columnar water vapour. AODs at four wavelengths from 440 to 1,020 nm were obtained from AERONET and then extrapolated to all other wavelengths using the 'Angstrom exponent'[9]. Within each layer from 0 to 3 km, we used the measured vertical distribution of aerosol concentration to scale the column AODs to AODs for each layer. For validation of this procedure, the MACR values were compared with the measured absorption coefficient at $\lambda = 370$, 520 and 880 nm: the measured and MACR values were within 10% of each other. The columnar ozone was measured using a hand-held multi-spectral Sun photometer. The procedure for estimating uncertainty in the measured and simulated heating rates is explained in the Supplementary Information.

CALIPSO. This satellite carries the first polarization lidar in space with lasers operating at 532 and 1,064 nm (ref. 3). The polarization enables us to distinguish between spherical cloud particles and non-spherical aerosols such as dust and soot. In addition, the dual wavelengths are used to retrieve aerosol size.

CCM3 input for the ABC forcing. The Chung *et al.* aerosol forcing was used in the CCM3 simulations. They[14] used recent aerosol satellite data from the MODIS instrument on NASA's TERRA satellite and ground-based aerosol robotics network[25] as the basis for the aerosol optical depths and single scattering albedo; and then used a combination of NASA's aerosol assimilation model and small mode aerosol radii from MODIS to determine the anthropogenic fraction of the observed AODs and single scattering albedos. Using this global distribution of anthropogenic AODs and single scattering albedo, Chung *et al.* introduce this data in the MACR model with satellite climatology of clouds to derive reduction of solar radiation at the surface and the increase in atmospheric solar absorption due to ABCs for the period 2000–2003. These estimates[14] were restricted to 2000–2003 because the MODIS data were available for this period, as were the GOCART values for the anthropogenic fraction. But they assumed that the aerosol plume was contained between the surface to 3 km a.s.l.; this was based on the Indian Ocean Experiment[1] observations over the Arabian sea.

Derived trends for the 1950–2000 period. The ABC-induced temperature changes shown in this study were estimated by comparing the CCM3 simulations that used the imposed 2000–2003 forcing with the simulations that did not use the ABC forcing. We then use ref. 13 to conclude that the computed warming must have occurred during the period 1950–2000. This coupled ocean–atmosphere model study[13], restricted to southern Asia, used the emission data of ABC precursors (SO_2 and soot) from 1930 to 2002. They took the present-day forcing from observations and aerosol assimilation models (this procedure was followed by ref. 14) for the period 1995 to 1999; and scaled this forcing with the published data for soot and SO_2 emission rates (as a function of time) to derive a time-dependent forcing from 1930 to 2000. Their emission data and the derived atmospheric solar heating and dimming show that more than 90% of the forcing occurred after 1950 (figure 1 in ref. 13). Ref. 14 validated the simulated trend in dimming by comparing the trend with the observed solar radiation trends over India (see top panel of figure 2 in ref. 13).